



Design of highly transparent conductive optical coatings optimized for oblique angle light incidence

N. Nedelcu¹ · V. Chiroiu¹ · L. Munteanu¹ · I. Girip¹ · C. Rugina¹ · A. Lőrinczi² · E. Matei² · A. Sobetkii³

Received: 27 April 2021 / Accepted: 24 June 2021 / Published online: 3 July 2021
© The Author(s), under exclusive licence to Springer-Verlag GmbH, DE part of Springer Nature 2021

Abstract

In this paper, three deposition techniques are combined to create a window material with high average transmission at oblique angles of incidence. Spectrophotometry and ellipsometry measurements, respectively, yield the optical constants n and k . In contrast with other analyses on the subject, a high average transmission, higher than 91% in the 450–900 nm spectral range, is obtained at incident angles of 20–25°. The refractive index and extinction coefficient are determined by the Swanepoel method. The iterative optimization performed using the OpenFilters software leads to an antireflection (AR) multilayer with low reflection and high transmission. The surface quality of the films was characterized by scanning electron microscopy (SEM) and atomic force microscopy (AFM), which revealed compact, continuous, and smooth films.

Keywords Thin films · Scanning electron microscopy · Optical properties · OpenFilters

1 Introduction

Transparent conductive optical coatings with a wide band-gap are important materials for many optoelectronic applications requiring the thin layers deposited on glass-produced devices, including transparent conductors and anti-reflective layers. Also, a highly transparent conductive coating for oblique angles of incidence is obtained for the visible spectral range, used in aviation applications [1].

Indium tin oxide (ITO) has recently become a popular choice for glass coatings which offers superior electrical conductivity and optical transparency in the visible wavelength spectral range [2]. The transparency film is much more important than optical conductivity. Indium tin oxide deposited on glass has many uses, such as de-icing and heater applications [3], microscope slides [4], monolithic RFI filters, touchscreens, and other display technologies [5]. Methods like thermal evaporation, chemical vapors

deposition, sol–gel method, spray pyrolysis, DC or RF magnetron sputtering are used for ITO deposition. They are attractive techniques used in industry for many engineers in optical coating materials [6–8]. Kurdesau et al. studied the ITO layers obtained by RF and DC magnetron sputtering at room temperature. The high transparency (80–85%) in the visible wavelength range with a low surface's sheet resistance 25 Ω /sq at normal incidence angle is obtained by DC magnetron sputtering [9].

Yilin Sung et al. [1] have developed a highly transparent optical coating using a conductive layer (ITO) and AlSiO_2 deposited on Corning Willow Glass. The coating optimization was for angles 0°, 30° and 60° for visible spectral range. The values of the spectral transmission are between 60% and 97.2%. D. Zhang et al. designed and fabricated a SiO_x /ITO double-layer anti-reflective coating for heterojunction silicon solar cells: one with a single-layer AR coating of 71 nm ITO and one with a double-layer AR coating of 71 nm SiO_x and 53 nm ITO; the average reflectance from 300 to 1200 nm spectral range is between 17.39% and 21.03% [10]. The influence of the incident angle on the optical and electrical properties of the indium thin oxide thin layer was studied by Y. Zhong et al. [11]. The oblique angle optimization suggested that ITO films have more application possibilities by allowing their optical and electrical properties to be tailored. Particularly, the oblique angle deposition method

✉ N. Nedelcu
nicoleta_dulgheru@yahoo.com

¹ Institute of Solid Mechanics, Romanian Academy, 15
Constatin Mille, 010141 Bucharest, Romania

² National Institute of Materials Physics, 405A Atomistilor St.,
077125 IF Magurele, Romania

³ MGM Star Construct Ltd., Pancota St., 022773 Bucharest,
Romania

is extensively used to modify the film refractive index to improve other optical properties [12, 13].

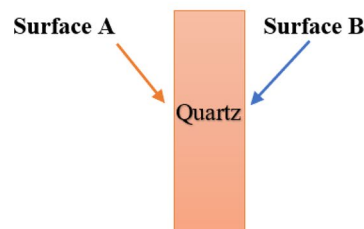
This paper reports a new window material with high average transmission, higher than 91% in the 450–900 nm spectral range at incident angles of 20–25°, which has been made using coated quartz glass. Both surfaces are coated with a sandwich layer structure. The optical properties, refractive index (n), extinction coefficient (k), and thickness (d) are determined by the Swanepoel method. Spectrophotometry measurements are correlated with ellipsometry measurements (SE) to compare the optical properties. OpenFilters software is used to optimize an antireflection layer, reduce the reflection factor, and increase the transmission of the optical glass component surfaces. The surface quality of the films was characterized by scanning electron microscopy (SEM) and atomic force microscopy (AFM), which revealed compact, continuous, and smooth films. XPS spectra proved very good chemical stability of the final MgF_2 layer of the complex AR coating. The surfaces are without cracks and digs, without exfoliation area.

2 Experimental procedure

A transparent conductive window with high transmission is obtained starting from quartz glass. Additional optimized layers were deposited layer by layer to achieve an average transmission higher than 91% in the spectral range of 450–900 nm at incident angles of 20–25°. To obtain a low reflection, antireflection layers are used. The structure of deposition for both surfaces is presented in Fig. 1. Three deposition methods are combined to obtain the highly transparent conductive window, as given by the following steps:

1. Pr_6O_{11} by thermal evaporation—control coating process—thin film thickness monitor quartz crystal microbalance.
2. ITO by sputtering DC in Ar/O_2 plasma—control coating process—by time with constant power.
3. $\text{MgF}_2 + \text{Ti}_3\text{O}_5$ by e-gun method—control coating process—optical monitoring systems, reflection measurement.

Fig. 1 The structure of layers deposition



The first method is thermal vacuum deposition, followed by DC sputtering. The powdered praseodymium oxide (Pr_6O_{11}) material of purity 99.9% was evaporated by the thermal vacuum deposition method. To establish the evaporation influence on the layer properties, the substrate temperature was changed from room temperature to 300 °C. In contrast, the evaporation speed ranged from 3 to 12 nm/min, and the O_2 total pressure was 1.2×10^{-2} Pa. This is a dielectric layer with a low thickness approach off 100 nm, especially used to increase the transmission in the final form of material.

DC sputtering is used to obtain the ITO layer. The ITO target has a dimension of $\phi = 150 \times 10$ nm. Before starting the ITO layer deposition, glow discharges took place, having a role in cleaning parts and activating the surface.

Working parameters are as follows: starting vacuum: 10^{-5} mbar; speed of rotation: 6 rpm; argon flow rate: 25 sccm; process vacuum: 10^{-3} mbar; power: 0.8 kW; process time: 30 min.

To avoid cracking or detachment of the cathode target, it is recommended that the deposition time be doubled with breaks (by disconnecting the power supply): 1 min deposition, 1 min pause (Fig. 2)

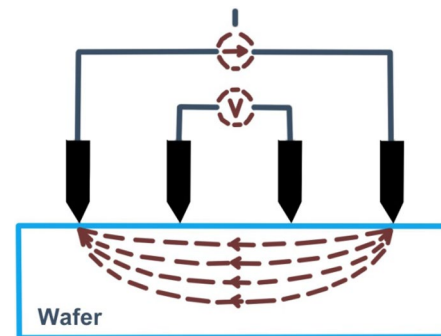
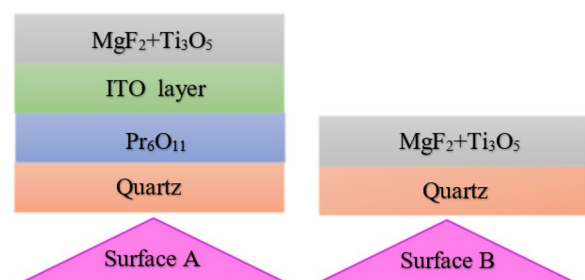


Fig. 2 Schematic of the four-point probe



3 Results and discussion

A 4-point probe (FPP) sheet resistance device is used to measure the ITO layer’s resistivity. Sheet resistance by 4-point probe is one of the most important properties for interconnect applications. It is also an important index to reflect the uniformity and purity of the deposited ITO layer.

The sheet resistance is measured by lowering the probe array to contact the central symmetric axis of the sample. To ensure the correct measurement, four different positions of each sample are measured. The measured resistance needs to be calibrated by two factors, named sample geometric correction factor, f_G , and instrument calibration factor, f_C :

$$R_s = R_m \times f_G \times f_C \tag{1}$$

where R_s is the sheet resistance, Ω/sq , and R_m is the measured sheet resistance, Ω/sq . The sample geometric correction factor, f_G , is used to correct the substrate edge effects. The correction is generally related to the ratio of the size (diameter for circle or length for square) of the wafer (D) divided by the probe spacing (S). The correction factor can be found in the FPP-100 operating manual (Veeco) [14]. The instrument calibration factor f_C , is used to correct the instrument disturbance, which is found by measuring the sheet resistance of a standard reference (Alfa Products, 99.999%) with an area of $2 \times 2 \text{ cm}^2$ and is obtained by dividing the bulk resistivity by the sheet resistance and thickness. To create a

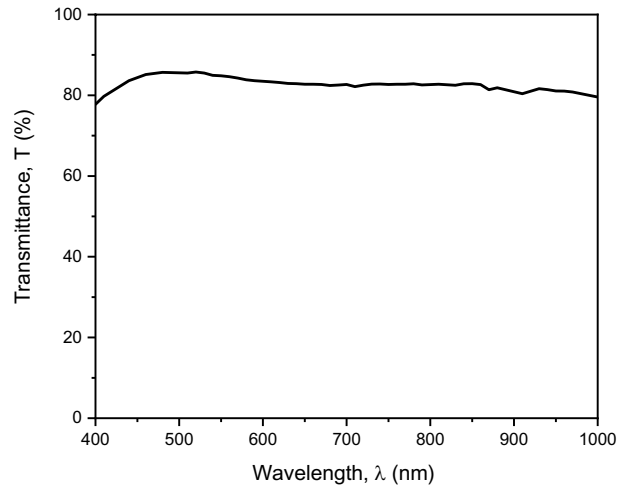


Fig. 3 The ITO transmission spectral for normal incidence for the layer with a sheet resistance of $30 \Omega/\text{cm}^2$

where n is the refractive index, s is the refractive index of the quartz substrate, d is thickness, and α is the absorption coefficient. The optical properties (n , k) and thickness (d) are determined by the Swanepoel method [15]. Applying the envelope function in spectral transmission gives maxima $T_M(\lambda)$ and minima $T_m(\lambda)$ for the whole wavelength range used to calculate the refractive index $n(\lambda)$, (Fig. 4) the thickness d and the absorption coefficient $\alpha(\lambda)$ (Fig. 5). The refractive index $n(\lambda)$ [15–20] is calculated by the relation:

$$n(\lambda) = \sqrt{2s \frac{T_M(\lambda) - T_m(\lambda)}{T_M(\lambda)T_m(\lambda)} + \frac{s^2 + 1}{2}} + \sqrt{\left(\frac{2s[T_M(\lambda) - T_m(\lambda)]}{T_M(\lambda)T_m(\lambda)} + \frac{s^2 + 1}{2}\right)^2 - s^2}, \tag{3}$$

linear distribution of thickness on time, we took into account a deposition time of 10 min doubled with breaks to determine the optical properties of the high-quality ITO layer. After deposition, the sheet resistance and spectra transmission were measured. The sheet resistance was found to be $30 \Omega/\text{cm}^2$. The optical transmission spectrum (Fig. 3) was recorded on Lambda 950 Spectrophotometer with double beam and double monochromator at room temperature, in the spectral range of 400–1000 nm, with 266 nm/min a scanning speed for normal incidences.

According to [15], the total transmission T is given by the relation (2):

$$T(\lambda) = \frac{16ns^2e^{-ad}}{(n + 1)^3(n + s^2) - 2\left[(n^2 - 1)(n^2 - s^2)\frac{4\pi nd}{\lambda}e^{-ad}\right] + (n - 1)^3(n - s^2)e^{-ad}}, \tag{2}$$

where $s = 1.458$ is given by

$$s = \frac{1}{T(\lambda)} + \sqrt{\left(\frac{1}{T(\lambda)^2} - 1\right)} \tag{4}$$

Figure 4 shows the variation of the refractive index n with the wavelength $\lambda[\text{nm}]$. The thickness d is around 335 nm and is calculated by the relation (3), (4):

$$d = \frac{\lambda_1 \lambda_2}{2(\lambda_1 n_2 - \lambda_2 n_1)} \tag{5}$$

The absorption coefficient $\alpha(\lambda)$ is obtained according to [13, 18] by the relation:

$$\alpha(\lambda) = \frac{1}{d} \ln \left[\frac{\left(\sqrt{Z + \sqrt{Z^2 - s^2}} - 1 \right)^3 \left(\sqrt{Z + \sqrt{Z^2 - s^2}} - s^2 \right)}{Y - \sqrt{Y^2 - (Z + \sqrt{Z^2 - s^2} - 1)^3 (Z + \sqrt{Z^2 - s^2} - s^4)}} \right], \tag{6}$$

where:

$$Z = \frac{2s(T_M(\lambda) - T_m(\lambda))}{T_M(\lambda)T_m(\lambda)} + \frac{s^2 + 1}{2}, \tag{7}$$

$$Y = \frac{8s^2[T_M(\lambda) - T_m(\lambda)]}{[T_M(\lambda)T_m(\lambda)]^2} [T_M(\lambda) - T_m(\lambda) + (s^2 - 1)T_M(\lambda)T_m(\lambda)] + \frac{4s[T_M(\lambda) - T_m(\lambda)]}{[T_M(\lambda)T_m(\lambda)]^2} \times \sqrt{\left(\frac{4s[T_M(\lambda) - T_m(\lambda)] + (s^2 + 1)T_M(\lambda)T_m(\lambda)}{2T_M(\lambda)T_m(\lambda)} \right)^2 - s^2}, \tag{8}$$

$n(\lambda)$, extinction coefficient $k(\lambda)$, and thickness d were evaluated from the spectro-ellipsometry analysis data. Figure 6

shows data analysis as a function of the ellipsometry angle $\psi(\lambda)$ (Fig. 6a) and $\Delta(\lambda)$ (Fig. 6b) versus wavelength λ . Spectro-ellipsometry analysis data were simulated by considering the samples as a two-layer optical system [substrate/first layer (film)/second layer (surface roughness)]. The optical

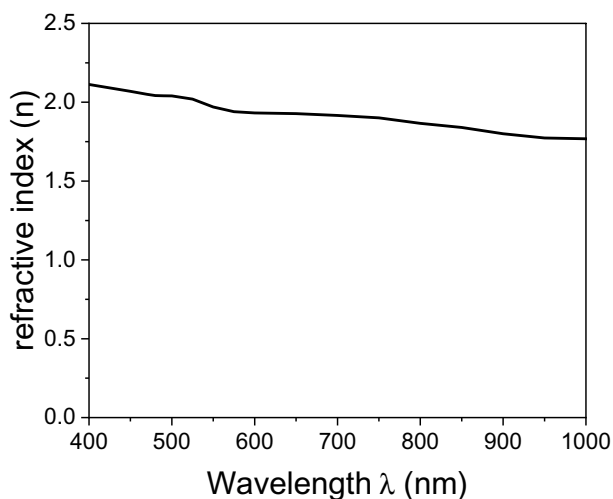


Fig. 4 The refractive index $n(\lambda)$ versus wavelength λ [nm]

with s the refractive index from the quartz [19, 20], and d is the thickness. The extinction coefficient $k(\lambda)$ is given by:

$$k(\lambda) = \frac{\lambda\alpha(\lambda)}{4\pi} \tag{9}$$

Figure 5 shows the variation of the absorption coefficient $\alpha(\lambda)$ and the extinction coefficient $k(\lambda)$.

The ellipsometry measurements were performed on a Variable Angle Spectroscopic Ellipsometer (VASE) (Woollam Co.) within the spectral range of 300–1700 nm at 55° angles of incidence. The optical parameters, refractive index

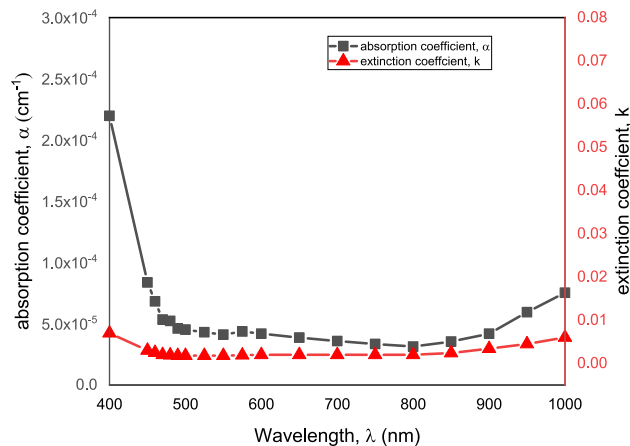


Fig. 5 The variation of the absorption coefficient $\alpha(\lambda)$ and the extinction coefficient $k(\lambda)$

constants (Fig. 7) were determined using Cauchy’s equation. The thickness obtained is around 333 nm. The results obtained by SE measurements are compared in Fig. 8 with the results calculated by UV–VIS–NIR spectroscopy. The comparison of the spectrophotometry data analysis with ellipsometry data analysis shows that the value for optical properties is the same; a small increase is observed for optical properties determinate by spectroscopy ellipsometer. The film thickness (d) and the optical constants (n and k) were obtained with an accuracy of ± 2 nm and ± 0.05 .

Our goal is to obtain a conductive layer (ITO) with 15 Ω/cm^2 sheet resistance. The ITO layer with 30 Ω/cm^2

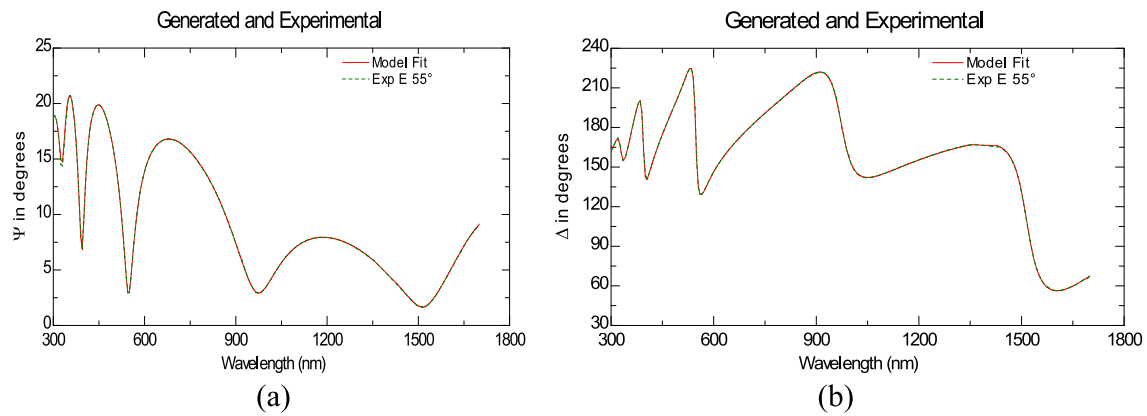


Fig. 6 The function of the ellipsometry angle $\psi(\lambda)$ **(a)** and $\Delta(\lambda)$ **(b)** versus wavelength λ

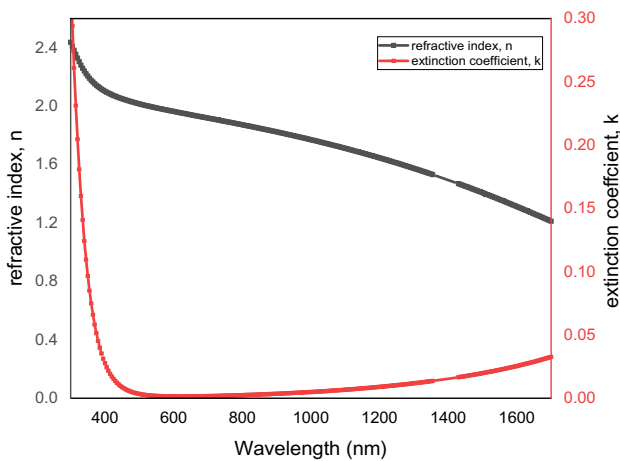


Fig. 7 The optical constants are determined by spectro-ellipsometry data analysis

sheet resistance was obtained at 10 min deposition time, doubled with breaks (by disconnecting the power supply): 1 min deposition, 1 min pause, keeping all working parameters the same, followed by the thermal treatment. The results obtained by spectrophotometry correlated with spectro-ellipsometry analyses; data show that the method used needs to be changed a little bit to achieve the goal. To decrease the sheet resistance and increase the thickness, it is necessary to modify the deposition time. First, we increase the deposition time at 20 min, doubled with breaks (by disconnecting the power supply): 1 min deposition, 1 min pause, keeping all working parameters the same, followed by the thermal treatment. The sheet resistance of the ITO layer deposited was $23 \Omega/\text{cm}^2$. It was necessary to increase the deposition time by 30 min following the steps described above. Figure 9 shows the diagram of

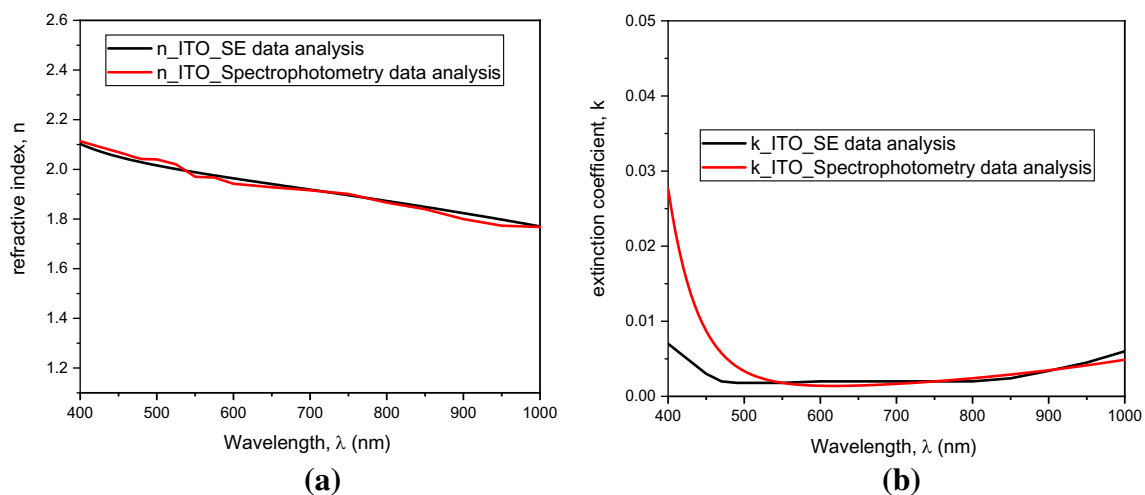


Fig. 8 The comparison of optical properties obtained by spectro-ellipsometry and spectrophotometry data analysis: **a** refractive index, **b** extinction coefficient

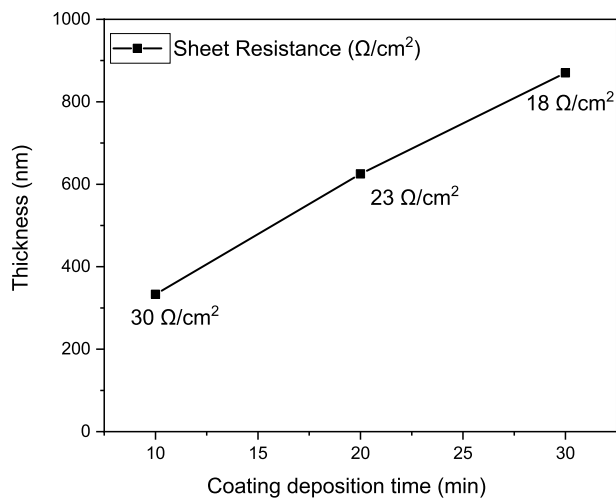


Fig. 9 The diagram of coating's thickness versus the deposition time for the ITO layer

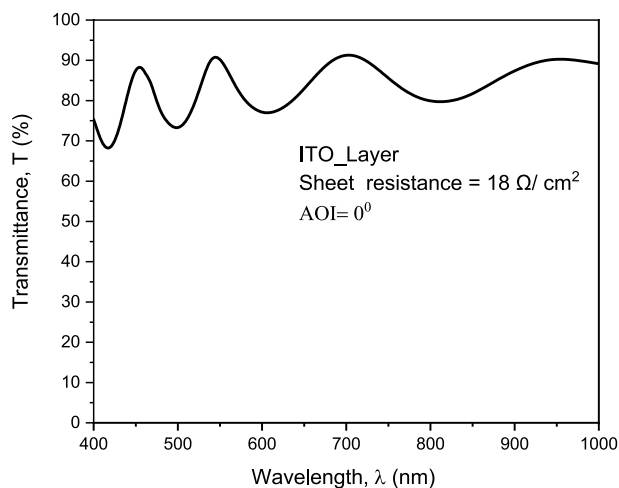


Fig. 10 The ITO transmission is spectral for normal incidence with sheet resistance $18 \Omega/\text{cm}^2$

Table 1 The coating parameters, estimated by OpenFilters

No	Film	d, nm
1	Ti_3O_5	25 ± 0.1
2	MgF_2	31 ± 0.1
3	Ti_3O_5	100 ± 0.1
4	MgF_2	12 ± 0.1
5	Ti_3O_5	46 ± 0.1
6	MgF_2	124 ± 0.1

coating deposition time versus the thickness. The result obtained showed that the sheet resistivity decreases with increase in the thickness. After deposition, the transmission spectra and sheet resistance are measured and presented in Fig. 10.

After all parameters (deposition time, sheet resistance, and thickness) have been established on quartz support covered with Pr_6O_{11} , the ITO layer was deposited with $15 \Omega/\text{cm}^2$ sheet resistance, for surface A. OpenFilters is a specially developed software for optical engineering, to design a new coating material. OpenFilters has a data-bank of materials and their optical properties, which can be updated with new materials by the user [19–25].

The Ti_3O_5 and MgF_2 materials are optimized for the spectral range of 450–900 nm at incident angles of 20–25°. The antireflection layer created is coated on *surface A* over the ITO and (Pr_6O_{11}) and *surface B*. The resulting antireflection coating consists of 6 thin layers. The parameters of the coating estimated by OpenFilters are shown in Table 1. The layers that form the antireflection coating are obtained by the e-gun method. The theoretical spectral reflection factor is shown in Fig. 11a, while the spectral reflection obtained experimentally is present in Fig. 11b.

The quality and durability of the layers have been tested using the MIL-C-48497A US Military Standards [26] for optical coatings, as follows:

Temperature: All films were exposed to $-62^\circ\text{C} + 72^\circ\text{C}$ for 24 hours; the temperature increase was 1°C per minute.

Humidity: The thin layers were exposed to $+49^\circ\text{C}$ and relative humidity 95–100% for 24 hours.

Adhesion: An adhesive tape (scotch tape) is firmly pressed onto the surface and quickly removed from the surface [27].

Salt solubility: The samples will be in a saline solution for 24 hours. Saline solution is prepared using 170 grams of salt NaCl per 3.8 liters of distilled water.

After immersion, we verified the surface coating, and no evidence of flaking, peeling, cracking, or blistering has been found.

Water solubility: The samples are tested immersed in distilled water for 24 hours.

All the samples were wiped with a cloth dipped in acetone and inspected with a magnifying glass and free of peeling marks. After performing the above-mentioned quality standard tests, all films were measured and characterized by scanning electron microscopy (SEM) and atomic force microscopy (AFM). The transmission experimental spectra measured at incidence angles of 21, 23, and 25° are presented in Fig. 12.

The thin film's surface morphology before and after the quality test was investigated by SEM (Figs. 13 and 14) and AFM (Figs. 15 and 16). They revealed compact, continuous, and smooth films. The surfaces are without cracks and digs, without exfoliation area, and consistent with the quality test results.

Following the quality standard tests performed on the surfaces of the thin films, one observes that the protrusions present initially on the surfaces diminished after the quality

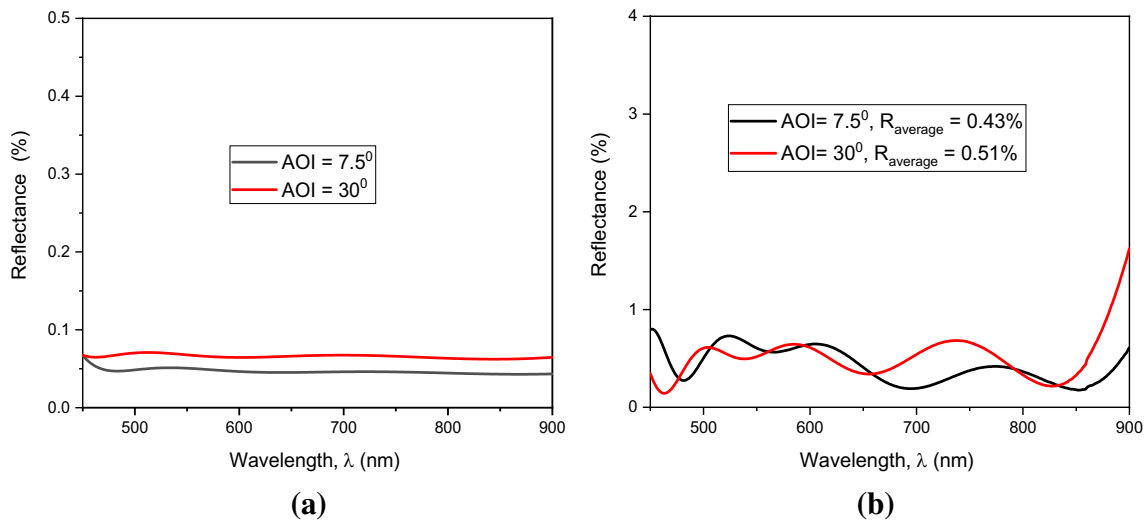


Fig. 11 Antireflection coating for the spectral range 450–950 nm optimized for angle of incidence, AOI=0–30°, **a** calculated by OpenFilters, **b** obtained experimentally by Spectrophotometer Lambda 950

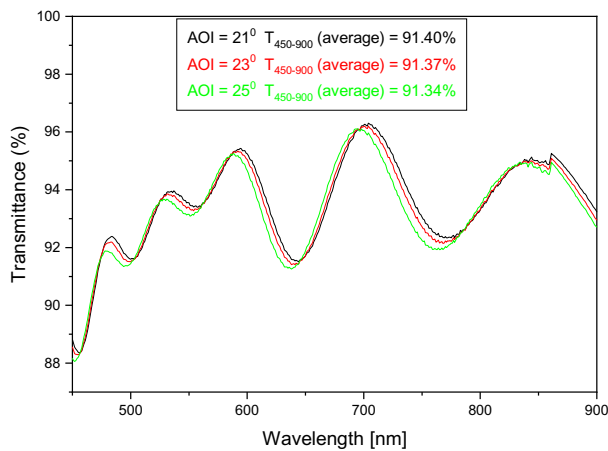


Fig. 12 The experimental transmission spectra were obtained after optimization

tests. The film becomes homogenous, presenting fine granulation of the surface (Figs. 13 and 14). This has happened most probably due to removed impurities (dust) from the film’s surface during the tests.

To check the chemical stability of the last coating layer from the AR multilayer structure, we performed x-ray photoelectron spectroscopy (XPS) analysis for the MgF₂ coating before and after the tests. The XPS measurement was carried out with a SPECS XPS spectrometer having a monochromatic Al K_α (1486.7 eV) X-ray source, operated at a power of 300 W. The pass energy was 20 eV for the spectra of the individual lines.

Table 2 summarizes the surface atomic concentrations in atomic percentage for the C, O, Mg, and F atomic species, before and after the test, estimated from the XPS measurements.

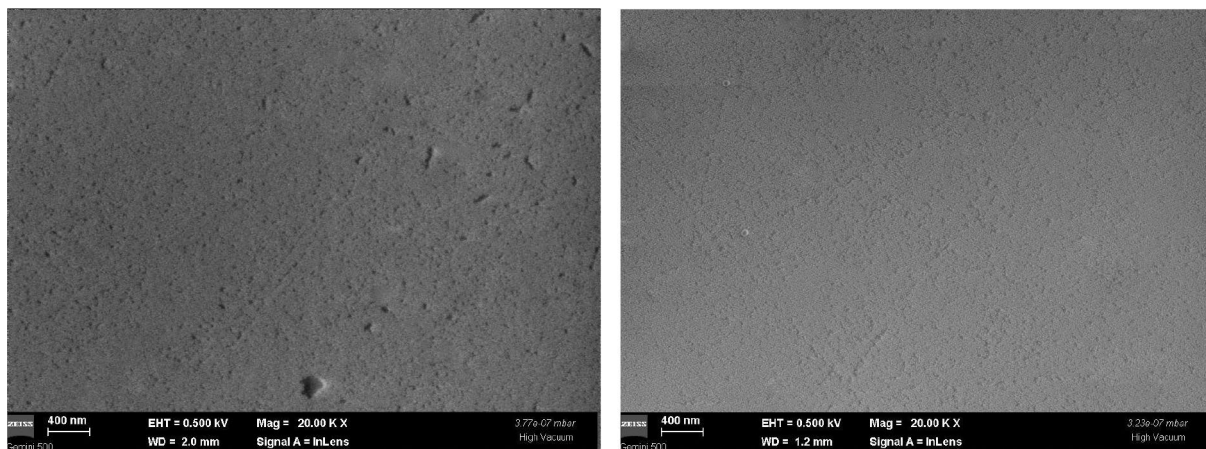


Fig. 13 The SEM images for surface A before and after the quality test

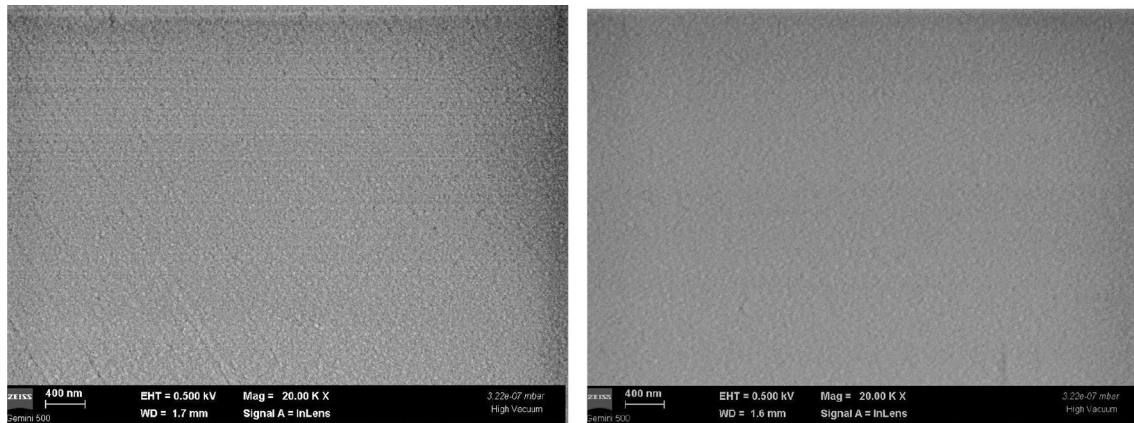


Fig. 14 The SEM images for surface B before and after the quality test

Fig. 15 The AFM images for surface A before and after the quality test

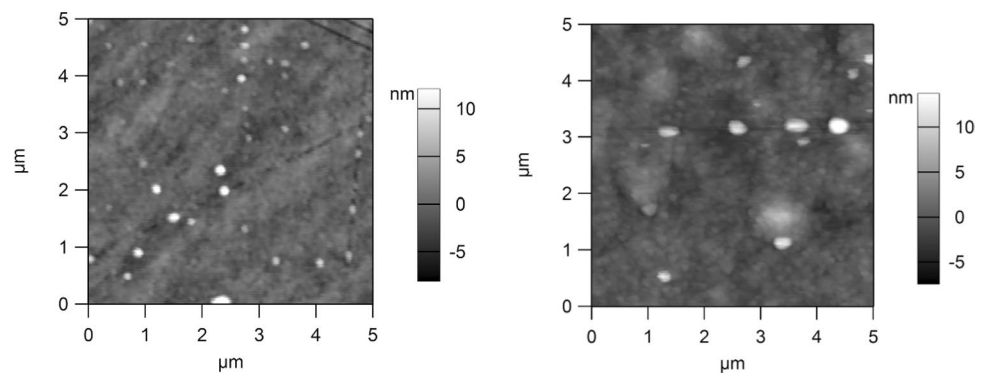


Fig. 16 The AFM images for surface B before and after the quality test

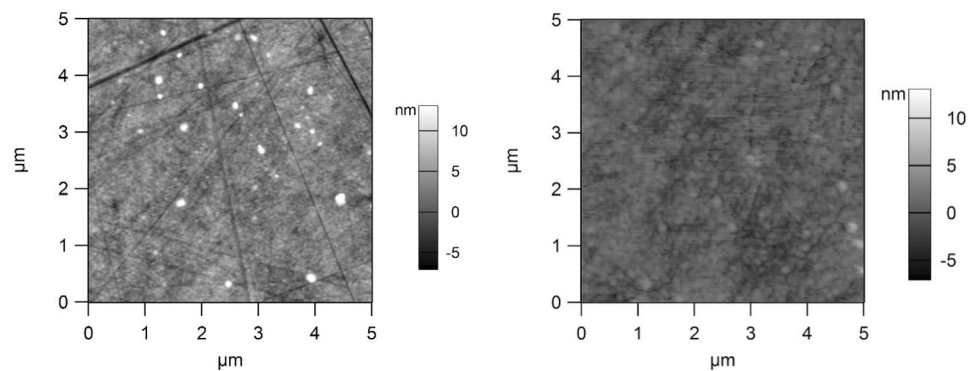


Table 2 Surface atomic concentrations (atomic %)

Sample	C	O	Mg	F
Before test	33.7	9.3	25.1	31.9
After test	34.8	7.4	24.8	33.1

Figures 17, 18, 19 and 20 show the superposed individual XPS line spectra before and after the test for the surface A, for the selected elements C, O, Mg, and F. While Mg and

F are the main components of the MgF_2 surface layer, the C and O are present mostly as contaminants of the surface.

We may observe that the line spectra for C, O, Mg and F are almost identical, which means very good chemical stability of the last MgF_2 layer during the tests. A somewhat larger difference of 0.2 eV shift which we have only in the case of the Mg2p line spectra, is due to surface morphology changes after the tests.

Fig. 17 The C1s line spectra before and after the test

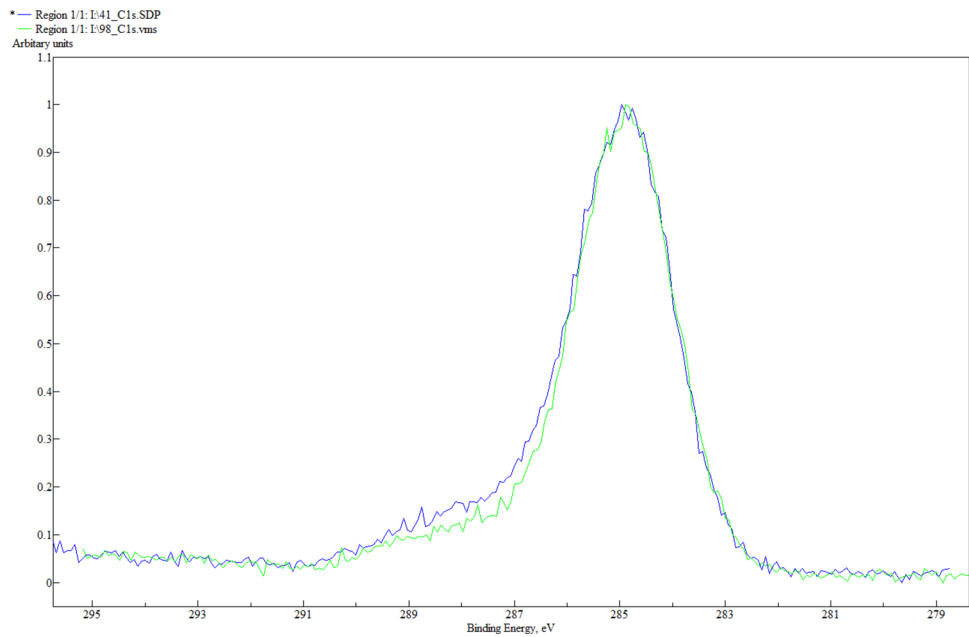
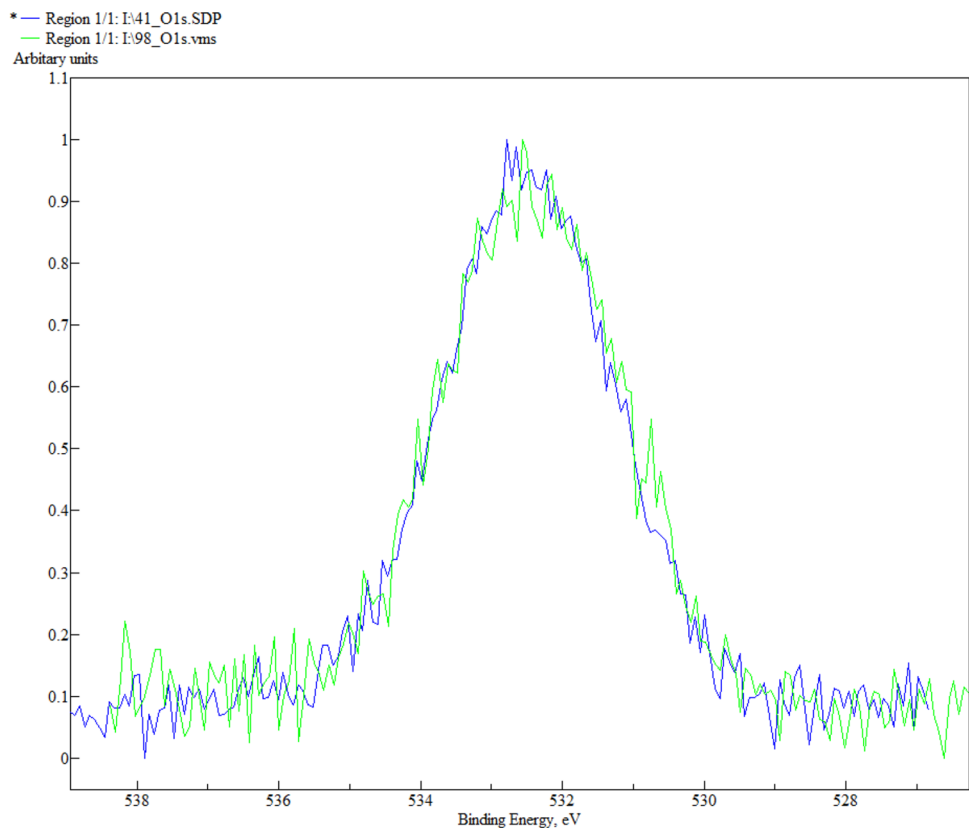


Fig. 18 The O1s line spectra before and after test



4 Conclusions

Three deposition techniques are combined to create a new window material with high transmission, more than 91% average for oblique angles of incidence. The conductive

layer (ITO) is characterized by ellipsometry and spectrophotometry methods to determine the optical constants and establish a $15 \Omega/\text{cm}^2$ sheet resistance. OpenFilters software is used to design a complex antireflection layer.

Fig. 19 Mg2p line spectra before and after the test

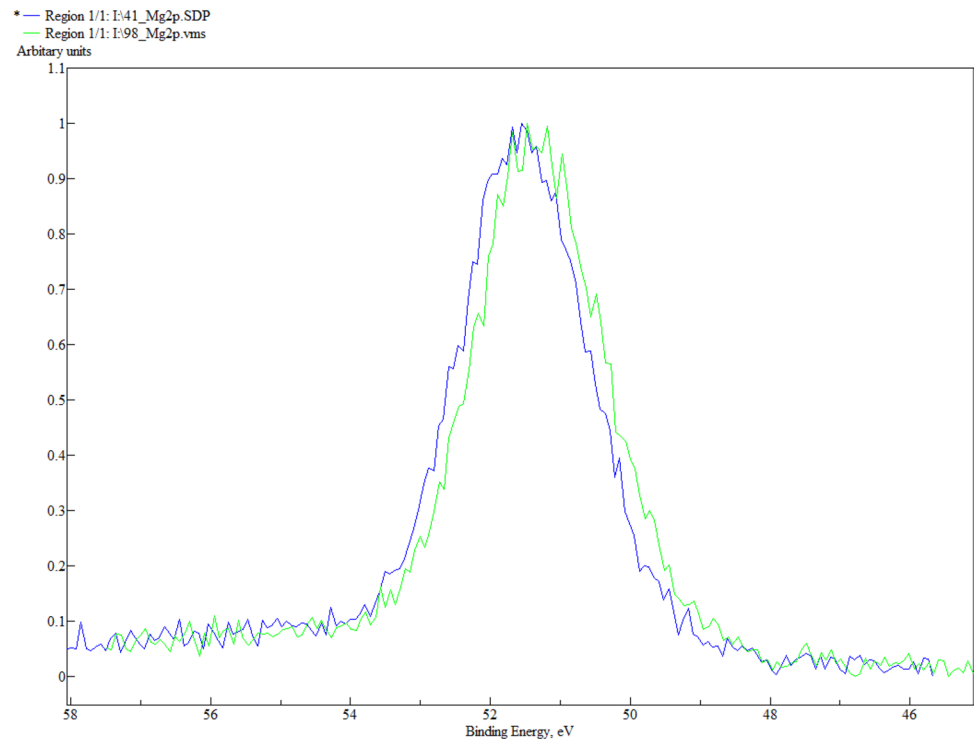
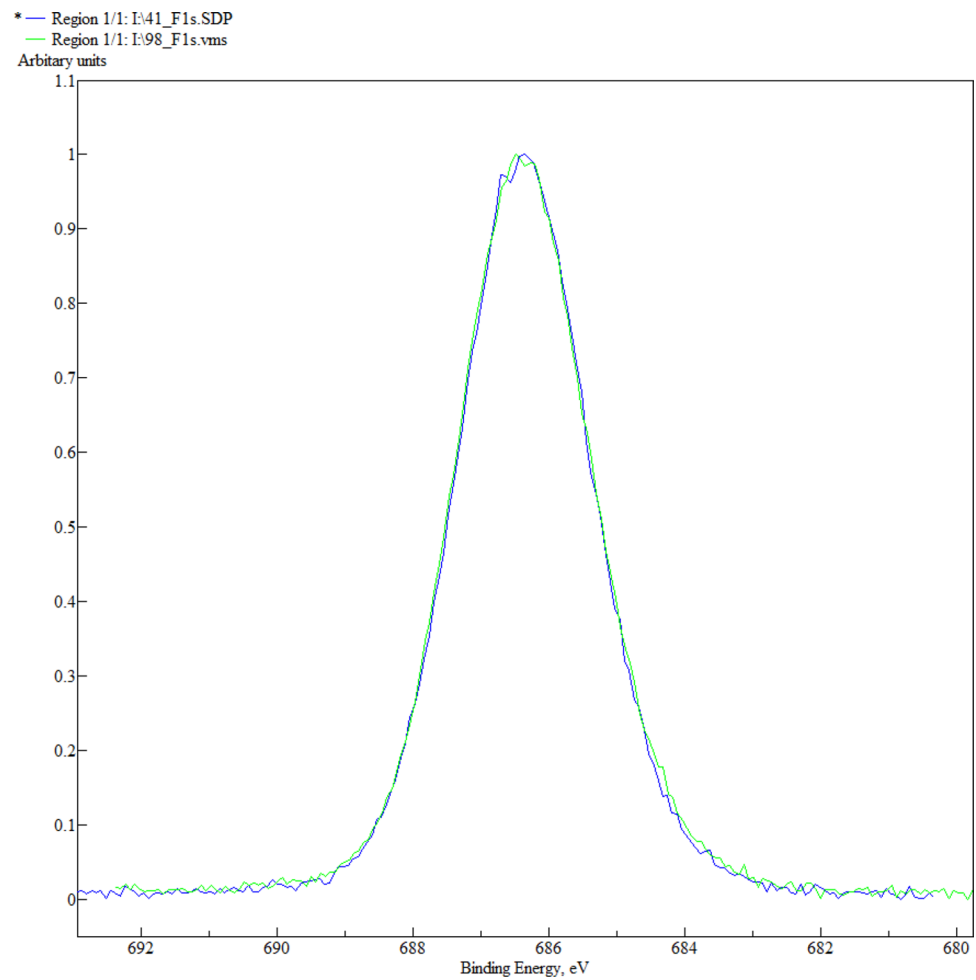


Fig. 20 F1s line spectra before and after the test



SEM and AFM analysis before and after quality tests revealed compact, continuous, and polycrystalline films. The root mean square (RMS) roughness of the sample surfaces measured before and after quality standard test by AFM was 1.56 nm (surface A) and 1.04 nm (surface B), and 1.75 nm (surface A) and 2.54 (surface B), respectively. XPS spectra proved very good chemical stability of the final MgF₂ layer of the complex AR coating. The surfaces are without cracks and digs, without exfoliation area.

A highly transparent conductive coating for the oblique angle of incidence is obtained in the visible spectral range, which might be used in aviation applications. The results may provide a better understanding of highly transparent conductive optical coatings for oblique angles of incidence.

Acknowledgements This work was supported by a grant from the Romanian Ministry of Education and Research, Project PN-III-P2-2.1-PED-2019-0085 CONTRACT 447PED/2020 for Institute of Solid Mechanics, Romanian, and through the Core Program 21N/2019 for National Institute of Materials Physics. The authors thank Dr. Constantin Logofătu and Dr. Cătălin Negrilă from NIMP for the XPS measurements and also Dr. Lucian Trupină for AFM measurements.

References

1. Y. Sung, R.E. Malay, X. Wen, C.N. Bezama, V.V. Soman, M.H. Huang, S.M. Garner, D.M. Poliks, D. Klotzkin, Anti-reflective coating with a conductive indium tin oxide layer on flexible glass substrates. *Appl. Opt.* **57**(9), 2202–2207 (2018)
2. I. Hamberg, C.G. Granqvist, Evaporated Sn-doped In₂O₃ films: Basic optical properties and applications to energy-efficient windows. *J. Appl. Phys.* **60**, R123 (1986)
3. N. Karim, M. Zhang, S. Afroj, V. Koncherry, P. Potluri, K.S. Novoselov, Graphene-based surface heater for de-icing applications. *RSC Adv.* **8**(30), 16815 (2018)
4. H. Pluk, D.J. Stokes, B. Lich, B. Wieringa, J. Fransen, Advantages of indium–tin oxide-coated glass slides in correlative scanning electron microscopy applications of uncoated cultured cells. *J. Microsc.* **233**(3), 353–363 (2009)
5. G. Walker, A Review of technologies for sensing contact location on the surface of a display. *J. Soc. Inf. Disp.* **20**(8), 413–440 (2012)
6. C. Guillén, J. Herrero, Structure, optical, and electrical properties of indium tin oxide thin films prepared by sputtering at room temperature and annealed in air or nitrogen. *J. Appl. Phys.* **101**, 073514 (2007)
7. J.-K. Kim, J.-M. Lee, Electrical and optical properties of near UV transparent conductive ITO/Ga₂O₃ multilayer films deposited by RF magnetron sputtering. *Appl. Phys. Lett.* **109**, 172107 (2016)
8. M.J. Alam, D.C. Cameron, Optical and electrical properties of transparent conductive ITO thin films deposited by sol-gel process. *Thin Solid Films* **377**, 455–459 (2000)
9. F. Kurdesau, G. Khripunov, A.F. da Cunha, M. Kaelin, A.N. Tiwari, Comparative study of ITO layers deposited by DC and RF magnetron sputtering at room temperature. *J. Non-Cryst. Solids* **352**(9–20), 1466–1470 (2006)
10. D. Zhang, I.A. Digdaya, R. Santbergen, R.A.C.M.M. van Swaaij, P. Bronsveld, M. Zeman, J.A.M. van Roosmalen, A.W. Weeber, Design and fabrication of a SiO_x/ITO double-layer anti-reflective coating for heterojunction silicon solar cells. *Solar Energy Mater. Solar Cells* **117**, 132–138 (2013)
11. Y. Zhong, Y.C. Shin, C.M. Kim, B.G. Lee, E.H. Kim, Y.J. Park, K.M.A. Sobahan, C.K. Hwangbo, Y.P. Lee, T.G. Kim, Optical and electrical properties of indium tin oxide thin films with tilted and spiral microstructures prepared by oblique angle deposition. *J. Mater. Res.* **23**, 2500–2505 (2008)
12. X. Yan, F.W. Mont, D.J. Poxson, M.F. Schubert, J.K. Kim, J. Cho, E.F. Schubert, Refractive-Index-Matched Indium–Tin-Oxide Electrodes for Liquid Crystal Display. *J. Appl. Phys.* **48**, 120203 (2009)
13. J.K. Kim, T. Gessmann, E.F. Schubert, J.Q. Xi, H. Luo, J. Cho, C. Sone, Y. Park, GaInN light-emitting diode with conductive omnidirectional reflector having a low-refractive-index indium-tin oxide layer. *Appl. Phys. Lett.* **88**, 013501 (2006)
14. K. Bautista, Four point operation, thin film deposition, (2004)
15. R.J. Swanepoel, Determination of the thickness and optical constants of amorphous silicon. *J. Phys. E: Sci. Instrum.* **16**, 1214–1222 (1980)
16. N. Nedelcu, V. Chiroiu, C. Rugină, L. Munteanu, R. Ioan, I. Girip, C. Dragne, Dielectric properties of GeSbSe glasses prepared by the conventional melt-quenching method. *Results Phys.* **16**, 12856 (2020)
17. N. Nedelcu, V. Chiroiu, L. Munteanu, I. Girip, Characterization of GeSbSe thin films synthesized by the conventional melt-quenching method. *Spectrosc. IR Spectrosc. Today's Spectrosc.* **35**, 22–33 (2020)
18. M. Gholami, A. Nazari, K. Azarin, S. Yazdanimeher, B. Sadeghniya, Determination of the thickness and optical constants of metal oxide thin films by different methods. *J. Basic. Appl. Sci. Res.* **3**(5), 597–600 (2013)
19. J. Sanchez-Gonzalez, A. Diaz-Parralejo, A.L. Ortiz, F. Guiberteau, Determination of optical properties in nanostructured thin films using the Swanepoel method. *Appl. Surf. Sci.* **252**, 6013–6017 (2006)
20. K. Salwan, I. Ali-Ani, Methods of determining the refractive index of thin solid films. *J. Appl. Phys.* **4**(1), 17–23 (2008)
21. D. Poitras, S. Larouche, L. Martinu, Design and plasma deposition of dispersion-corrected multiband rugate filters. *Appl. Opt.* **41**, 5249–5255 (2002)
22. Y. Wen, P. He, Y. Yao, Y. Zhang, R. Cheng, L. Yin, N. Li, J. Li, J. Wang, Z. Wang, Bridging the van der Waals interface for advanced optoelectronic devices. *Adv. Mater.* **32**(7), 1906874 (2019)
23. W. Yan, C. Dong, Y. Xiang, S. Jiang, A. Leber, G. Loke, W. Xu, C. Hou, S. Zhou, M. Chen et al., Thermally drawn advanced functional fibers: new frontier of flexible electronics. *Mater. Today* **35**, 168–194 (2020)
24. Q. Ou, X. Bao, Y. Zhang, H. Shao, G. Xing, X. Li, L. Shao, Q. Bao, Band structure engineering in metal halide perovskite nanostructures for optoelectronic applications. *Nano Mater. Sci.* **1**, 268–287 (2019)
25. S. Larouche, L. Martinu, Open-source software for the design, optimization, and synthesis of optical filters. *Appl. Opt.* **47**(13), C219–C230 (2008)
26. Coating, single or multilayer, interference: *durability requirements specification* – (1980) - MIL-C-48497 Revision A
27. N. Nedelcu, V. Chiroiu, L. Munteanu, C. Rugina, Uncertainties of transmittance and absorbance measurements of the chalcogenide thin films. *Appl. Phys. A* (2021). <https://doi.org/10.1007/s00339-021-04297-z>

Publisher's Note Springer Nature remains neutral with regard to jurisdictional claims in published maps and institutional affiliations.